

Synthesis of nanocast ordered mesoporous carbons and their application as electrode materials for supercapacitor

Wen-Cui Li · Gu-Zhen Nong · An-Hui Lu ·
Hao-Quan Hu

Published online: 31 December 2009
© Springer Science+Business Media, LLC 2009

Abstract Various nanocast ordered mesoporous carbons (OMCs) were synthesized using mesoporous silicas such as SBA-15, SBA-16, KIT-6, SBA-3 and MCM-48 as templates via nanocasting pathway. The structures of OMCs were analyzed by X-ray diffraction, transmission electron microscope and nitrogen sorption technique. These OMCs with well-defined pore structure were used as model electrode materials for investigating the influence of pore structure on their double layer capacitances. The cyclic voltammetry and galvanostatic charge/discharge measurements were conducted to estimate the capacitive behaviour of OMCs. The results show that the mesopore structures of OMCs play an important role in improving surface utilization for the formation of electrical double layer. OMCs synthesized from SBA-15 and SBA-16 show great advantage over others because their micropores are being easy accessible through the mesopores, thus allowing rapid electrolyte ion diffusion. To achieve a higher specific capacitance ($\mu\text{F cm}^{-2}$), the optimized amount ratio between micropore and mesopore needs to be controlled. In addition, great impact of the electrode disc thickness on the capacitive performance was demonstrated by a series of careful measurements.

Keywords Nanocasting · Ordered mesoporous carbons · Pore structure · Electric double-layer capacitor · Electrode disc thickness

1 Introduction

Supercapacitors offer a promising alternative approach to meeting the increasing power demands of energy storage systems in general [1]. Carbon-based supercapacitors, which are mainly based on the accumulation of charges in electrical double layer without faradaic reaction, bridge the gap between batteries and conventional dielectric capacitors, and are ideal for rapid storage and release of energy. For instance, they can be coupled with lithium batteries or fuel cells to provide power peaks during acceleration as well as for energy recovery during braking of electric vehicles [2].

As known, for carbon materials, their porous structures including specific surface areas [3], pore sizes [4], functional groups [5], and orientation of graphene layers [6] highly affect the double layer capacitance for supercapacitors. The formation of electrical double layer is remarkably efficient in carbon pores with the size below 1 nm because of lacking of space charge and a good attraction of ions along the pore walls [7–9]. Chmiola et al. [10] found an anomalous increase in capacitance for self-synthesized carbide-derived carbons with unimodal micropores smaller than 1 nm. However, for good dynamic charge propagation, smaller mesopores are useful, especially in the cases of using non-aqueous electrolytes [7]. It is therefore believed that high surface area carbons with a well-balanced micro- and mesoporosity could be potentially more advantageous than solo microporous carbons concerning the improvement of power density [11–13].

Nanocast ordered mesoporous carbons (OMCs) are particularly interesting as electrode materials for supercapacitors in terms of both fundamental research and practical application. OMCs usually present very narrow

W.-C. Li (✉) · G.-Z. Nong · A.-H. Lu · H.-Q. Hu
State Key Laboratory of Fine Chemicals, Dalian University of
Technology, 116012 Dalian, China
e-mail: wenculi@dlut.edu.cn

pore size distribution, well-defined pore arrangement, large surface area and good electrical conductivity. These porous parameters are tunable by varying the synthetic conditions such as by selecting desired hard templates, carbon precursors and carbonization parameters. Using OMCs as the electrode materials, it may potentially provide an insight into the relationship between porous structure and capacitive behaviour of carbon in a supercapacitor. Jurewicz et al. reported a study of using OMCs templated from SBA-15 and MCM-48 as electrode materials for supercapacitors. They found out that OMC from MCM-48 displayed high capacitance ($F\ g^{-1}$) due to the remarkable microporous character, meanwhile the mesopores allowed easier ion diffusion to the active surface [11]. Fuertes et al. [12] investigated the capacitance behaviour of two OMCs templated from SBA-16 with variable pore sizes. They concluded that mesopores with 3 nm in size were sufficiently useful for perfect ions motion, and the amount of micropores mainly determined the values of capacitance. In contrary, Sevilla et al. [14] pointed out that mesopores of OMCs did not significantly improve the ionic mobility as compared with the micropores (pore sizes between 1.0 and 1.3 nm) of activated carbons.

Up to date, most of the studies mainly focus on the discussion of pore size effect of OMCs on their capacitive performance. Recently, Li et al. [15] investigated the possible influence of other factors related to the pore depth of OMCs on the electrochemical performance. In their study, OMC with much shorter pore depth of 200–300 nm was synthesized using a kind of short-axis-orient-growth SBA-15 as the template. Such OMC showed an improved capacitance of $14\ \mu F\ cm^{-2}$ in 6 M KOH solution. Under identical conditions, only $10\ \mu F\ cm^{-2}$ of capacitance was achieved for similar OMC but with longer pore depth on micrometer level. The superior performance of short pore length OMC was attributed to the enhanced electrolyte accessibility of pores and a short pathway for rapid ion diffusion [15]. Inspired by this work, we consider that besides the pore length, most likely, the pore structure (the manner of pore arrangement) may also affect, to some extent, the electrochemical performance of OMCs. Therefore, in the present study, a series of OMCs with various pore structure were synthesized via nanocasting pathway in aiming to investigate the influence of the pore structure on double layer capacitance. For that, at the first step, the impact of the electrode disc thickness on capacitance was carefully investigated. A suitable electrode disc thickness was applied for all the measurements thus to exclude the potential influence derived from the variance in testing conditions.

2 Experimental

2.1 Preparation of silica templates and OMCs

According to the previous reports, ordered mesoporous silicas including SBA-3 [16], SBA-15 [17], KIT-6 [18], MCM-48 [19], and SBA-16 [20] were synthesized and their properties were compiled in Table 1. Mesoporous silicas SBA-3 and SBA-15 have two-dimensional hexagonal pore ordering with same space group of *p6mm*, but with different pore sizes and pore wall thicknesses. Both KIT-6 and MCM-48 display three-dimensional cubic structure (*Ia3d*) but with different pore sizes and pore wall thicknesses. In addition, SBA-16 has a body-centred cubic cage structure, whose space group is *Im3 m*. Using these silicas as the templates, OMCs with variable pore structure but with closer mesopore sizes can be synthesized. In this way, we can study the effects of pore structure of OMCs on their electrical performances.

OMCs were prepared via nanocasting pathway [21]. Briefly, furfuryl alcohol as carbon precursor was impregnated into the pores voids of silica templates by incipient wetness in the presence of oxalic acid. The molar ratio between furfuryl alcohol and oxalic acid is of 200:1. The impregnated sample was cured in air at 90 °C for 2 days, thus furfuryl alcohol was converted to polyfurfuryl alcohol. After polymerization, the sample was then carbonized at 850 °C for 2 h under N₂ atmosphere. OMCs was obtained after dissolution of silica template in NaOH solution (1 M), followed by filtration, washing, neutralized with HNO₃ (0.1 M) and drying steps. Elemental analyses show that the amount of silicon residue in the OMCs is neglectable.

2.2 Characterization of the porous structure of OMCs

The low-angle powder X-ray diffraction (XRD) was performed on a Rigaku D/Max-2400 X-ray diffractometer

Table 1 Structure parameters of silica templates used in this study

Sample	Space group	S _{BET} ($m^2\ g^{-1}$)	V _{tot} ($cm^3\ g^{-1}$)	D _{max} (nm)
KIT-6	<i>Ia3d</i>	765	1.13	6.2
MCM-48	<i>Ia3d</i>	1246	0.86	2.2
SBA-15	<i>p6 mm</i>	723	1.02	6.2
SBA-3	<i>p6 mm</i>	961	1.09	3.7
SBA-16	<i>Im3 m</i>	930	0.81	7.3

S_{BET}: apparent surface area calculated by BET method; V_{tot}: total pore volume at p/p₀ = 0.995; D_{max}: pore size with a maximum in the pore size distribution based on the desorption branch, and for SBA-16 based on the adsorption branch

(Cu K α radiation, $\lambda = 1.5432 \text{ \AA}$). Transmission electron microscopy (TEM) analyses were carried out with Tecnai G²20S-Twin equipment operating at 200 kV. The samples for TEM analysis were prepared by dipping the carbon-coated copper grids into the ethanol solutions of the porous carbons ultrasonic treated for 20 min with 40 kHz and 150 W. The porous parameters of OMCs were characterized by nitrogen sorption technique at 77 K using a Micromeritics ASAP 2020 analyser. Samples were degassed at 200 °C for at least 6 h prior to determination of the isotherms. The specific surface area and pore size distribution were analyzed by Brunauer–Emmett–Teller (BET) theory and Barrett–Johner–Halenda (BJH) method, respectively. The maximum value on the pore size distributions was referred as the pore diameter. The total pore volume was estimated from the amount adsorbed at the relative pressure of 0.995. The micropore volume and mesopore volume were estimated by using α_s -plot method [22, 23]. The reference adsorption isotherm used in α_s -plot calculation was reported elsewhere [24].

2.3 Electrochemical measurements

OMCs were crushed into fine powder and mixed with certain amount of polytetrafluoroethylene (PTFE) as the binder with the weight ratio (OMC/PTFE) of 19:1. The mixture was pressed on a nickel foam current collector. The area and the mass of each electrode disc were controlled at about 1 cm² and 10 ± 2 mg, respectively. Cyclic voltammetry (CV) measurements were carried out using a conventional three electrode system with a platinum plate and saturated calomel electrode (SCE) as the counter and reference electrode, respectively. CV curves were recorded by polarizing the working electrode between 0 and –0.8 V versus chloridized argentine in a 6 M KOH aqueous solution with a scan rate of 5 mV s^{–1} on a CHI602C electrochemical workstation. The galvanostatic charge/discharge measurements were conducted at 1 mA g^{–1} of current density between 0 and 1 V in two-electrode constructed cell using carbon as cathode and anode. The specific capacitance C_g (F g^{–1}) was determined by the equation $C_g = I\Delta t/V$ from the discharge profile, where Δt (s) is the discharging time, V(V) is the potential range from the end of charge to the end of discharge except ohmic drop, I (mA g^{–1} or mA cm^{–2}) is the applied specific current based on the total mass or surface area of OMC in both electrodes. Before electrochemical tests, the electrodes were impregnated with electrolyte for 24 h. All the measurements were conducted at room temperature.

3 Results and discussion

3.1 Impact of the electrode disc thickness on the capacitance

Developing high performance carbon materials as electrodes for supercapacitors is a rapidly growing field. However, one problematic issue is that comparison of capacitances of similar carbon materials from different laboratories is often difficult because of the large variance in testing conditions. Among many parameters, the thickness or mass of the as-prepared electrode disc is the most difficult one to be controlled identically in different batches. In our experiments, OMC named as MC-KIT-6 templated from KIT-6, and resin-based microporous activated carbon (AC), were prepared as electrode discs with identical area of 1 cm² but with variable mass. Accordingly, the thickness of the electrode disc was varied. The more carbon material used, the thicker the electrode disc is. The nitrogen isotherms of MC-KIT-6 and AC were displayed in Fig. 1a. The galvanostatic charge/discharge measurements were conducted to determine their specific capacitance. As shown in Fig. 1b, specific capacitance was plotted against electrode mass. Essentially, the capacitances of these two carbons are varying in a similar way. That is, the capacitance increases with the decrease of electrode mass. Especially, when the electrode mass is less than 10 mg, the capacitance dramatically increases. Most likely, no matter using microporous or mesoporous carbon, the thinner the electrode disc is, the higher the capacitance will be. A small vibration of electrode mass in the range of few milligrams can cause a big jump of the capacitance value. These results indicate that the diffusion of electrolyte ions into a thicker electrode was obstructed to some extent, which results in a proportion of electrode surface being electrochemically inaccessible. From these experiments we learned that that thinner electrode resulted in higher capacitance. More importantly, to ensure the obtained capacitances are comparable, the electrodes should be made with similar thickness. In the following study, we tried to keep our electrode discs prepared with identical thickness, that is to say, the mass of each electrode was fixed in the range of 10 ± 2 mg.

3.2 Influence of pore structure on the capacitive behavior

In order to investigate the influence of the pore structure on capacitive behavior of OMCs, three kinds of OMCs were first prepared using mesosilica SBA-15, KIT-6 and SBA-16 as the hard templates, and furfuryl alcohol as the carbon source. The obtained carbons were accordingly denoted as

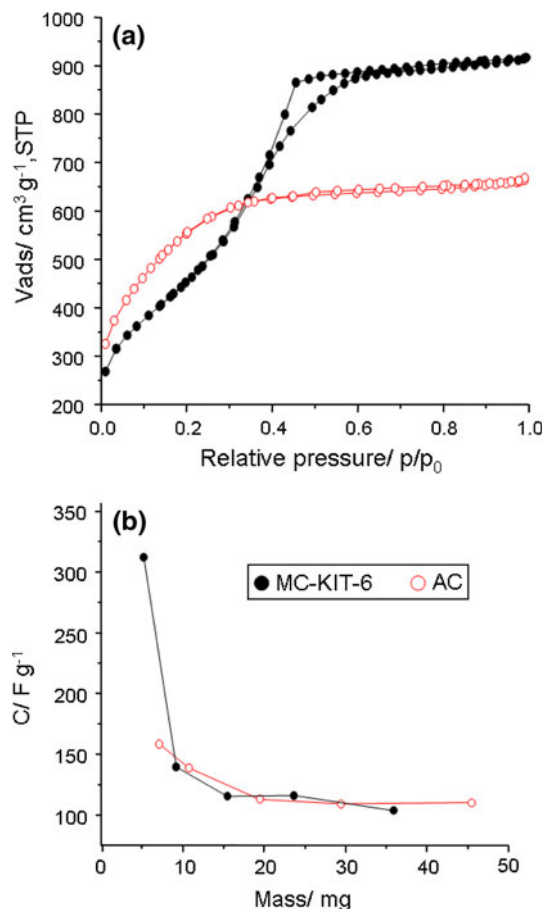


Fig. 1 **a** N_2 sorption isotherms of MC-KIT-6 (S_{BET} : $1657\text{ m}^2\text{ g}^{-1}$, V_{tot} : $1.42\text{ cm}^3\text{ g}^{-1}$) and AC (S_{BET} : $2027\text{ m}^2\text{ g}^{-1}$, V_{tot} : $1.02\text{ cm}^3\text{ g}^{-1}$) and **b** Relation between electrode mass and specific capacitance

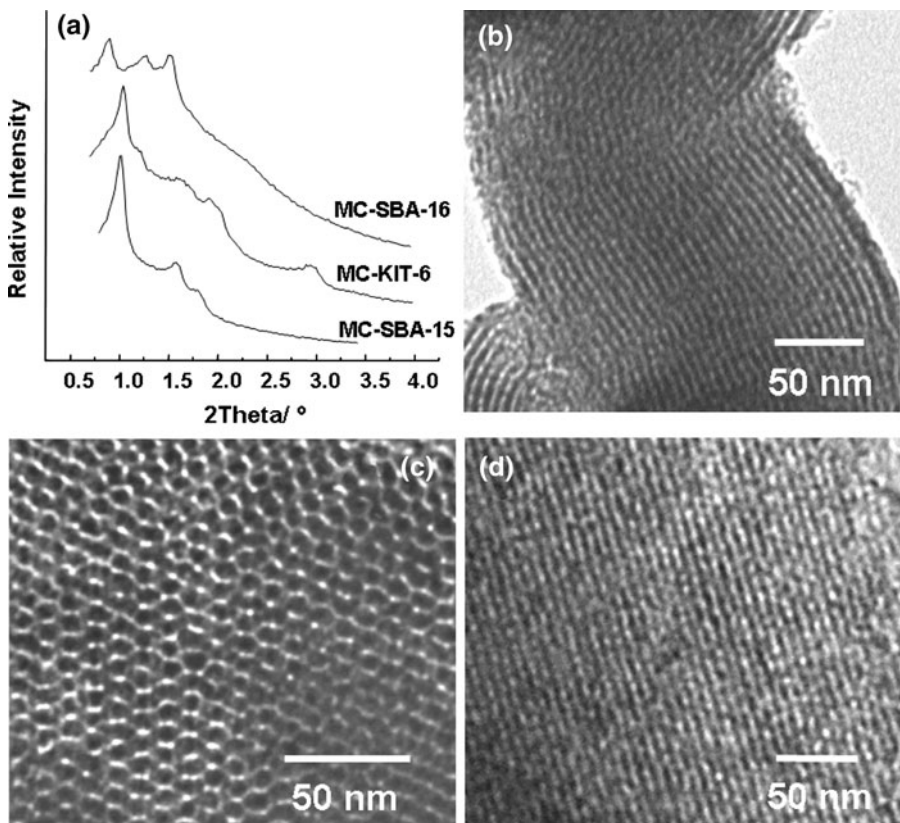
MC-SBA-15, MC-KIT-6, and MC-SBA-16. It is noteworthy that same carbon precursor used to prepare OMCs guarantees surface chemistry as same as possible. Thus wettability and even pseudocapacity caused by the use of different carbon precursors will be negligible. The low-angle XRD patterns of the obtained OMCs were shown in Fig. 2a. The clear reflections of MC-SBA-15 can be assigned to *p6 mm* space group, indicating two-dimensional hexagonal pore ordering in this carbon, whereas the XRD patterns of MC-KIT-6 and MC-SBA-16 can be indexed to three-dimensional cubic structure with space group of *Ia3d* and body-centred cubic cage structure with space group of *Im3 m*, respectively. TEM images further confirm these OMCs having highly ordered structures. As shown in Fig. 2b, a clear two-dimensional hexagonal ordered structure can be observed in MC-SBA-15, whilst MC-KIT-6 presents a three-dimensional cubic periodic structure (Fig. 2c). The sideway viewed TEM micrographs of MC-SBA-16 also show well-ordered channels (Fig. 2d). These prepared carbons almost perfectly replicated the structure of the silica templates.

Nitrogen sorption isotherms and the corresponding pore size distributions of the resultant carbons were presented in Fig. 3a, b. As can be seen in Fig. 3a, the nitrogen sorption isotherms are quite similar and essentially of type IV with a pronounced hysteresis loops, indicating that these carbons all exhibit mesoporous feature. The steep capillary condensation steps in the isotherms suggest narrow pore size distributions of these carbons. As can be seen from Fig. 3b, the pore size distributions of these carbons are very concentrated. MC-SBA-15, MC-KIT-6 and MC-SBA-16 display a maximum in the pore size distribution curves around 3.3, 3.4 and 3.7 nm, respectively. These values are quite close to each other. The calculated porous parameters were compiled in Table 2. Due to inapplicability of t-plot method in calculating micropore surface area and pore volume of OMCs, a comparison plot (α_s -plot) introduced by Gregg and Sing [22], later on developed by Setoyama et al. [23] and Centeno et al. [25], was employed to determine the micropore and mesopore volumes. These values are more reliable than those obtained from t-plot, but absolute values still have to be interpreted with care.

Cyclic voltammogram (CV) tests were performed at a scan rate of 5 mV s^{-1} in a three-electrode cell for evaluation of these OMCs' capacitive behaviors. The recorded CV plots were shown in Fig. 4a. Essentially, MC-KIT-6 and MC-SBA-16 show similarly CV curves close to rectangular, despite the different pore structure they have. Differently, the CV curve of MC-SBA-15 is much close to rectangle shape for a charge-discharge cycle as compared to that of MC-KIT-6 or MC-SBA-16. Such small difference may arise from the straight pore channels existed in MC-SBA-15, which benefits a relatively rapid charge-discharge process in double-layer capacitance.

The typical galvanostatic charge-discharge behavior performed in two-electrode configuration was shown in Fig. 4b. Clearly, they all exhibit triangle-like symmetry charge-discharge profiles and good linear galvanostatic charge-discharge curves without obvious ohmic drop. That indicates these OMCs possess a good capacitive character under the present loading current density. However, a visible difference in the slope of the discharge plot is observed, reflecting the specific capacitances are different among these three OMCs. The calculated capacitances were listed in Table 2. It can be seen that MC-SBA-16 presents a relatively high mass specific capacitance (F g^{-1}) as compared to that of MC-KIT-6, though the BET surface areas and pore sizes of both carbons are almost identical. The imageable difference between MC-SBA-16 and MC-KIT-6 is the pore structure, which is most likely responsible for the difference of mass specific capacitances. MC-SBA-15 exhibits a relative low capacitance, which is due to its low surface area. According to the commonly accepted assumption that the capacitance (expressed as the

Fig. 2 XRD patterns (a), and TEM images of MC-SBA-15 (b), MC-KIT-6 (c) and MC-SBA-16 (d)



unit of $F\text{ g}^{-1}$) is proportional to the specific surface area of electrode materials, we thus convert mass specific capacitance to surface specific capacitance (expressed as the unit of $\mu\text{F cm}^{-2}$). It turns out to be that the capacitances varied in the sequence of MC-KIT-6 < MC-SBA-15 < MC-SBA-16. As known, SBA-16 template has body-centred cubic cage-like $I\bar{m}3\bar{m}$ structure with 8 apertures around a cage [26]. Its carbon replica exhibits a similar structure as that of SBA-16 after nanocasting process, as also confirmed by the XRD pattern in Fig. 2a. MC-SBA-15 shows similar pore structure as that of its parent template, i.e. two-dimensional hexagonal symmetry structure and straight pore channel. MC-KIT-6 has three-dimensional cubic pore geometry and its mesopore channels are twisted. Judging from the surface specific capacitance ($\mu\text{F cm}^{-2}$), one can conclude that the straight porous channels of MC-SBA-15 reasonably allow easy and quick charge-discharge as compared to the twisted ones of MC-KIT-6. Jurewicz et al. [9] have found a linear relationship between capacitance and micropore volume. Larger micropore volume always leads porous carbon to a high capacitance. To ensure micropore surface areas are available to a great extent for forming electrical double layer, the micropores should be directly interconnected to mesopores [11]. As seen in Table 2, the micropore volume of MC-SBA-15, MC-KIT-6, and MC-SBA-16 are comparable. The obvious differences in capacitances ($\mu\text{F cm}^{-2}$) are most likely arising from the intrinsic pore

structure of MC-SBA-15, MC-KIT-6 and MC-SBA-16. In terms of easy accessibility of micropores through mesopores, the pore structure of MC-SBA-15 and MC-SBA-16 are more favorable than that of MC-KIT-6. Thus, at a fixed loading current density, the straighter the open porous channels are, the higher the capacitance ($\mu\text{F cm}^{-2}$) will be.

Besides aforementioned silica SBA-15, KIT-6, and SBA-16, mesoporous silica SBA-3 and MCM-48 were also employed as the hard templates to replicate mesoporous carbons for further investigation of the role of pore structure. The replicated carbons were named as MC-SBA-3 and MC-MCM-48. The XRD patterns, nitrogen sorption isotherms, and the pore size distributions of MC-SBA-3 and MC-MCM-48 were correspondingly shown in Fig. 5a, b, c. Their textural parameters can be found in Table 2.

As seen in Fig. 5a, the low-angle XRD pattern indicates that MC-MCM-48 doesn't show the $I\bar{a}3d$ structure as its parent template MCM-48 has, but converted to a new cubic $I\bar{4}1/a$, as suggested previously [27]. In principle, MC-SBA-3 should display the $p6\text{ mm}$ ordered structure as MC-SBA-15 has. However, a relatively weak ordered structure in MC-SBA-3 is observed, possibly due to a small pore size and weak interconnectivity in the pore walls of mother SBA-3, which causes reduction of ordered structure after nanocasting process [28]. Their sorption isotherms (Fig. 5b) are still of type IV with a small hysteresis, indicating a mesoporous feature. As seen in Fig. 5c, the mesopore sizes of MC-SBA-3

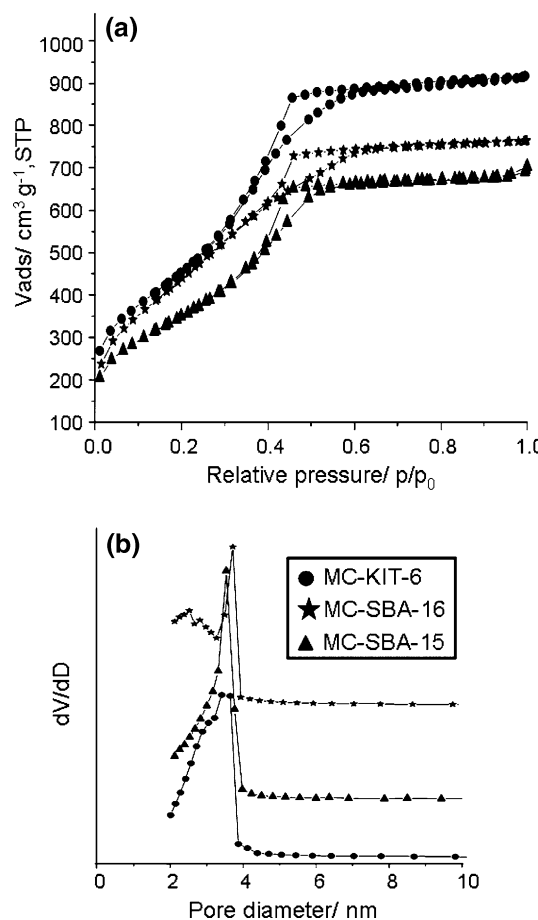


Fig. 3 **a** N_2 sorption isotherms and **b** pore size distributions of mesoporous carbons

and MC-MCM-48 are concentrated around 3.6 nm and 3.4 nm, respectively. Both carbons display very high BET surface area (see Table 2).

Figure 6a displayed the obtained CV curves of MC-SBA-3 and MC-MCM-48. Compared to MC-MCM-48, the CV curve of MC-SBA-3 is relatively close to rectangle shape, which is similar to that of MC-SBA-15. In addition, the galvanostatic charge–discharge plots were shown in Fig. 6b. Both curves present triangle-like symmetry charge–discharge profiles, similar to that of MC-SBA-15 and MC-KIT-6, demonstrating that these mesoporous

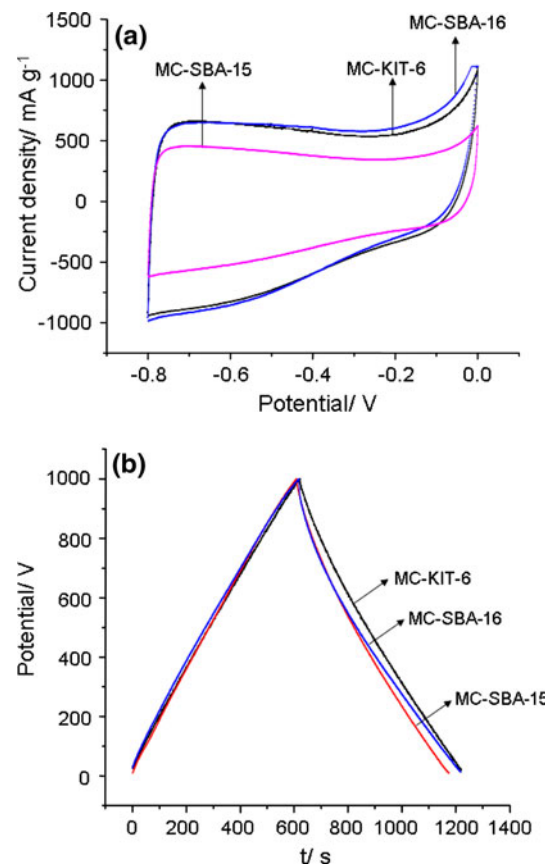


Fig. 4 CV curves **(a)** and galvanostatic charge–discharge profiles **(b)** of OMCs in 6M KOH aqueous solution

carbons have good capacitive character. As can be seen in Table 2, MC-SBA-3 shows higher mass specific capacitance (F g^{-1}) than that of MC-SBA-15, which is due to its high specific surface area. A similar phenomenon is also observed in the cases of MC-KIT-6 and MC-MAM-48. Nevertheless, when the mass specific capacitance (F g^{-1}) is converted to surface specific capacitance ($\mu\text{F cm}^{-2}$), it turns out to be that the capacitances of MC-SBA-3 and MC-MCM-48 are correspondingly lower than those ones of MC-SBA-15 and MC-KIT-6. By comparing the textural parameters, one can figure out that the microporosities of MC-SBA-3 and MC-MCM-48 are accordingly higher than that of MC-SBA-15 and MC-KIT-6. Obviously, in these

Table 2 Textural parameters and capacitances of nanocast ordered mesoporous carbons

Sample	S_{BET} ($\text{m}^2 \text{g}^{-1}$)	V_{tot} ($\text{cm}^3 \text{g}^{-1}$)	V_{meso} ($\text{cm}^3 \text{g}^{-1}$)	V_{micro} ($\text{cm}^3 \text{g}^{-1}$)	D_{max} (nm)	C (F g^{-1})	C^* ($\mu\text{F cm}^{-2}$)
MC-SBA-15	1135	0.92	0.33	0.52	3.3	112	9.9
MC-KIT-6	1657	1.42	0.69	0.66	3.4	144	8.7
MC-SBA-16	1638	1.18	0.53	0.59	3.7	176	10.8
MC-SBA-3	1889	1.11	0.38	0.56	3.6	151	8.0
MC-MCM-48	2304	1.19	0.35	0.75	3.4	188	8.2

V_{meso} and V_{micro} : mesopore and micropore volumes calculated based on α_s -plot method. The others are the same as noted in Table 1

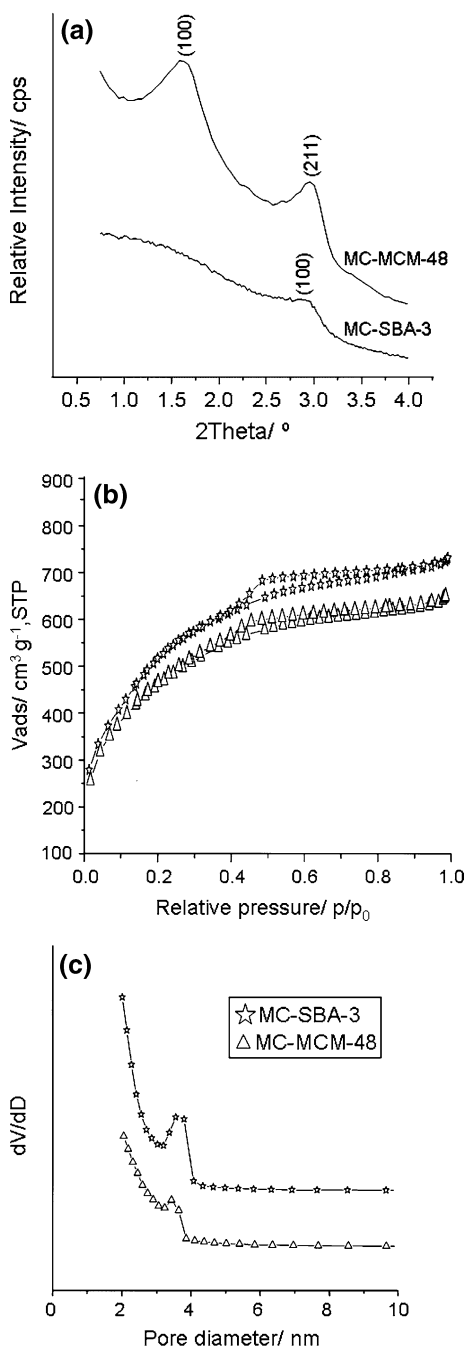


Fig. 5 **a** XRD patterns, **b** Nitrogen sorption isotherm, **c** Pore size distributions of MC-SBA-3 and MC-MCM-48

cases, not all micropores are electrochemically accessible. The surface area derived from micropores is not fully utilized for the contribution of double layer capacitance. In principle, MC-SBA-3 should have similar two-dimensional hexagonal ordered structure as that of MC-SBA-15. However, due to the small mesopore size of SBA-3 template, the porous channels of MC-SBA-3 might partially collapse after removal of silica template, so that the interconnectivity between micropores and mesopores might be

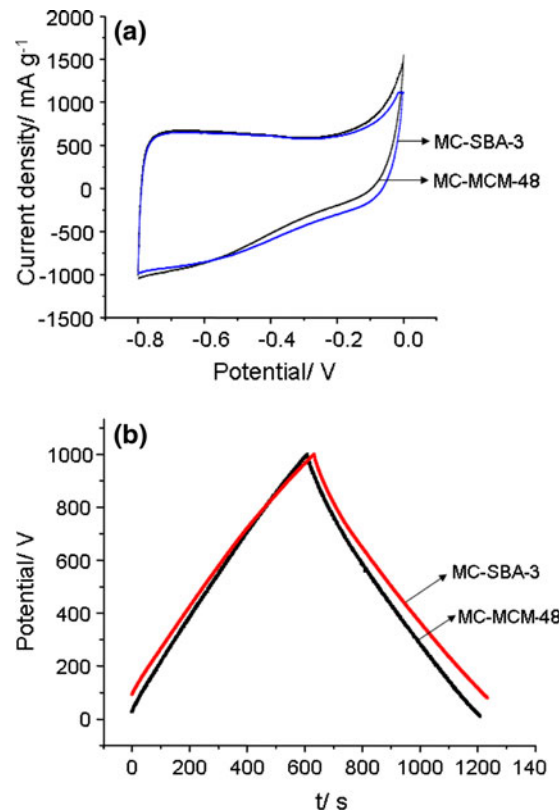


Fig. 6 **a** Cyclic voltammetry curves, and **b** Galvanostatic charge-discharge profiles of MC-SBA-3 and MC-MCM-48 performed in 6M KOH aqueous solution

blocked somehow. Thus, the accessibility of electrolyte ions through mesopores to micropores was reduced. The surface utilization of MC-MCM-48 is better than that of MC-SBA-3, due to the better maintained ordered structure. But still, the abundant micropores (micropore volume is double times higher than mesopore volume) are not fully available for the formation of electrical double layer in a three-dimensional cubic structure of MC-MCM-48. Clearly, the pore structure in OMCs should be considered as one of the crucial factors affecting the electrochemical performance of a porous carbon.

4 Conclusion

A series of OMCs with high surface area, narrow pore size distribution, and variable pore structure were synthesized using SBA-15, KIT-6, SBA-16, MCM-48 and SBA-3 as the hard templates. Using these OMCs as model electrodes, we found out that the mesopore structure have remarkable influence on the capacitive performance of OMCs. This should be considered an important issue for a supercapacitor. As results, the mesopore structure of MC-SBA-15 and MC-SBA-16 is more favorable than that of MC-KIT-6,

MC-MCM-48 and MC-SBA-3 in terms of the accessibility of micropores through mesopores, and the surface utilization for the formation of electrical double layer. Therefore, the enhancement of the capacitance for a porous carbon in supercapacitor is not only relying on high surface area, other factors such as the pore structure, pore size distribution, porous interconnectivity, etc., should be comprehensively considered as well. It is most likely that a porous carbon exhibiting high capacitive performance should have the following features, such as high surface area, electrochemically accessible micropores and mesopores, reasonable ratio between micropores and mesopores, better interconnectivity between pores, and more straight porous channels, etc. These factors affect the capacitive performance in a cooperative manner and probably have an optimum values in term of achieving ideal capacitance.

Acknowledgments This work is supported by Program for New Century Excellent Talents in University of Chinese Ministry of Education (NCET-08-0075). The authors would like to thank the basic funding provided by Max-Planck-Institut für Kohlenforschung (MPIKOFO), and Dalian University of Technology (DUT) funding for the DUT-MPIKOFO joint research center.

References

1. A.G. Pandolfo, A.F. Hollenkamp, *J. Power Sources* **157**, 11 (2006)
2. A. Chu, P. Braatz, *J. Power Sources* **112**, 236 (2002)
3. H. Shi, *Electrochim. Acta* **41**, 1633 (1996)
4. J. Chmiola, G. Yushin, R. Dash, Y. Gogotsi, *J. Power Sources* **158**, 765 (2006)
5. B.E. Conway, *Electrochemical Supercapacitors* (Plenum Press, New York, 1999), p. 186
6. C.H. Kim, S.I. Pyun, J.H. Kim, *Electrochim. Acta* **48**, 3455 (2003)
7. E. Frackowiak, *Phys. Chem. Chem. Phys.* **9**, 1774 (2007)
8. U. Fischer, R. Saliger, V. Bock, R. Retricevic, J. Fricke, *J. Porous. Mater.* **4**, 281 (1997)
9. H. Pröbstle, M. Wiener, J. Fricke, *J. Porous. Mater.* **10**, 213 (2003)
10. J. Chmiola, G. Yushin, Y. Gogotsi, C. Portet, P. Simon, P.L. Taberna, *Science* **313**, 1760 (2006)
11. K. Jurewicz, C.V. Guterl, E. Frackowiak, S. Saadallah, M. Reda, J. Parmentier, J. Patarin, F. Beguin, *J. Phys. Chem. Solids* **65**, 287 (2004)
12. A.B. Fuertes, G. Lota, T.A. Centeno, E. Frackowiak, *Electrochim. Acta* **50**, 2799 (2005)
13. H.Y. Liu, K.P. Wang, H. Teng, *Carbon* **43**, 559 (2005)
14. M. Sevilla, S. Alvarez, T.A. Centeno, A.B. Fuertes, S. Stoeckli, *Electrochim. Acta* **52**, 3207 (2007)
15. H.Q. Li, J.Y. Luo, X.F. Zhou, C.Z. Yu, Y.Y. Xia, *J. Electrochem. Soc.* **154**, A731 (2007)
16. Q. Huo, D. Margolese, G.D. Stucky, *Chem. Mater.* **8**, 1147 (1996)
17. D. Zhao, J. Feng, Q. Huo, N. Melosh, G.H. Fredrickson, B.F. Chmelka, G.D. Stucky, *Science* **279**, 548 (1998)
18. T.W. Kim, F. Kleitz, B. Paul, R. Ryoo, *J. Am. Chem. Soc.* **127**, 7601 (2005)
19. J.M. Kim, S.K. Kim, R. Ryoo, *Chem. Commun.* 259 (1998)
20. T.W. Kim, R. Ryoo, M. Kruk, K. Gierszal, M. Jaroniec, S. Kamiya, O. Terasaki, *J. Phys. Chem. B* **108**, 11480 (2004)
21. A.H. Lu, W.C. Li, W. Schmidt, W. Kiefer, F. Schüth, *Carbon* **42**, 2939 (2004)
22. S.J. Gregg, K.S.W. Sing, *Adsorption, Surface Area and Porosity* (Academic Press, New York, 1982), p. 94
23. N. Setoyama, T. Suzuki, K. Keneko, *Carbon* **36**, 1459 (1998)
24. M. Kruk, M. Jaroniec, K.P. Gadkaree, *J. Colloid Interface Sci.* **192**, 250 (1997)
25. T.A. Centeno, M. Sevilla, A.B. Fuertes, F. Stoeckli, *Carbon* **43**, 3012 (2005)
26. T.W. Kim, R. Ryoo, *J. Mater. Chem.* **15**, 1560 (2005)
27. M. Kaneda, T. Tsubakiyama, A. Carlsson, Y. Sakamoto, T. Ohsuna, O. Terasaki, *J. Phys. Chem. B* **106**, 1256 (2002)
28. F. Chen, X.J. Xu, S. Shen, S. Kawi, K. Hidajat, *Micropor. Mesopor. Mater.* **75**, 231 (2004)